Inverted Cucurbit[*n*]urils: Density Functional Investigations on the Electronic Structure, Electrostatic Potential, and NMR Chemical Shifts

Rahul V. Pinjari and Shridhar P. Gejji*

Department of Chemistry, University of Pune, Ganeshkhind, Pune 411007, India

Received: October 21, 2008; Revised Manuscript Received: December 4, 2008

Inverted cucurbit[*n*]uril (i^xCB[*n*], $x = 1, 2$; $n = 6-8$), the enantiomers of cucurbit[*n*]uril (CB[*n*]) comprising one or more inverted glycouril units, show distinct selectivity in recognition toward the guest by the virtue of shape and dimensions of its cavity. The *i*CB[*n*] ($x = 1$ and $n = 6, 7$) are isolated as intermediates during the synthesis of CB[*n*]. In this work, density functional theory using the hybrid B3LYP functional has been employed to derive the electronic structure and the NMR chemical shifts in the i^xCB[*n*] hosts. The present calculations have shown that the inversion of the glycouril unit of CB[6] and CB[7] engenders a destabilization by 4.2 and 5.7 kJ mol^{-1}, respectively, and, as opposed to this, the *i*CB[8] is favored by 18.6 kJ mol^{-1} over the corresponding CB[8] host. Likewise, i^2CB[7] possessing two inverted glycourils are highly destabilized over CB[7]. A large separation of the inverted glycouril units reduces the repulsion between methine protons inside the cavity, rendering the 1,4-i^2CB[*n*] ($n = 7$ or 8) to be of lowest energy. Stabilization energies from the self-consistent reaction field (SCRF) theory are calculated with water, ethanol, and tetrahydrofuran (THF) as solvents. Unlike in gas phase and other solvents, the stabilization hierarchy *i*CB[6] < *i*CB[7] < *i*CB[8] has been predicted in THF. Molecular electrostatic potential (MESP) was used to gauge the cavity shape of these hosts. Consequently the *i*CB[6] reveals a half-sprocket-like cavity; an additional tooth for each glycouril in the succeeding *i*CB[*n*] homologue was noticed. In the case of the 1,5-i^2CB[8] enantiomer, the cavity turns out to be rectangular. The deeper MESP minima near the ureido oxygens suggest strong electrostatic interactions with the guest at the *i*CB[6] portals. The electron-rich region within the cavity explains the large affinity of CB[*n*] toward the electron deficient guests. The electronic distribution and shape and size of the cavity thus derived provide insights for the inclusion of guests of different shapes in a variety of i^xCB[*n*] hosts. NMR chemical shifts have shown that the methylene protons near the inverted glycouril and the methine protons those are directing toward the cavity yield distinct signals, consistent with those observed in experiments. The protons within the cavity are less affected by solvation.

1. Introduction

Cucurbit[*n*]uril CB[*n*] ($n = 5-8$ or more) are cyclic methylene bridged glycouril oligomers that represent a fascinating class of molecules which are composed of a hydrophobic cavity surrounded by hydrophilic portals lined up with the polar ureido carbonyl groups.[1] Owing to the attributes of common depth but varying equatorial or annular widths, CB[*n*] offer stronger binding of different guests. The growing interest in this class of molecules mainly stems from its remarkable affinity and high selectivity toward the guest facilitated by the inner cavity of CB[*n*] and its opening. Electrostatic potential investigations have revealed that CB[*n*] portals are significantly more electron-rich than that of β-cyclodextrin.[2] This engenders an effective binding of guests ranging from acids, alcohols,[3,4] aromatic molecules,[5−13] ferrocene, cobaltocene[2,14−18] to peptides[19,20] within the CB[*n*] host. Consequently, CB[*n*] hosts are efficiently used in a variety of applications, namely, organic synthesis,[12,21−27] catalysis,[28−30] nanotechnology,[31,32] and supramolecular chemistry.[33−39] Syntheses and X-ray crystal structure of CB[*n*] ($n = 5-8$) homologues are reported.[33,40−42] Theoretical investigations on the CB[*n*] homologues and their derivatives and inclusion of guests within the CB[*n*] cavity have also been discussed in the literature.[43−48] Electronic structure, charge distribution, and NMR chemical shifts in the CB[*n*] ($n = 5-8$) and their host−guest complexes were investigated using the density functional theory by the present authors.[43]

Isaacs and co-workers[49−52] have recently studied the family of *i*CB[*n*] analogues wherein one of the glycouril units in CB[*n*] is inverted and thus the methine carbon and protons in this unit are directed inside the cavity. These *i*CB[*n*] were isolated as intermediates during the synthesis of CB[*n*] from the reaction of glycouril and formaldehyde in acidic media and were detected by ^{1}H NMR spectroscopy.[40−42] Single crystal data of *i*CB[6] and *i*CB[7][51] have suggested that the methine protons of the inverted glycouril unit placed within the cavity engender smaller cavity volume compared to their CB[*n*] counterpart. It is not surprising that the small cavity with open portals of *i*CB[6] and *i*CB[7] led to loose binding of guests with different selectivity compared to the CB[*n*] hosts. Further, the inverted glycouril rendered a large dipole moment to these *i*CB[*n*] enantiomers.[51] The inverting of one or two glycourils as in *i*CB[*n*] or i^2CB[*n*] influences significantly the hydrophobicity of the cavity as well as the hydrophilicity at the portals, which primarily governs interaction with the guest, that is, either accommodation within the cavity or lateral interaction with the portals. As a pursuance to understand the binding of the guest within the inverted-CB[*n*] cavity, the electronic structure, molecular electrostatic potential (MESP), and ^{1}H and ^{13}C NMR chemical shifts have been calculated. The relative stabilization of different i^xCB[*n*] enantiomers and the influence of solvent on the energies and the

* Corresponding author. E-mail: spgejji@chem.unipune.ernet.in.

10.1021/jp809293s CCC: $40.75
Published on Web 01/15/2009

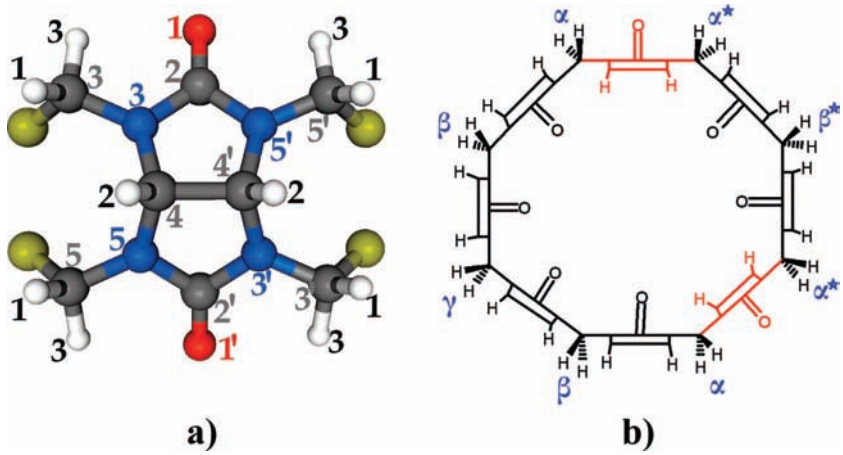

Figure 1. (a) Atom numbering scheme in the repeating unit of *i*[*n*]CB[*n*]. (b) Labels used for the symmetry equivalent atoms in 1,4-*i*[2]CB[8] as an example. Inverted glycourils are shown in red color.

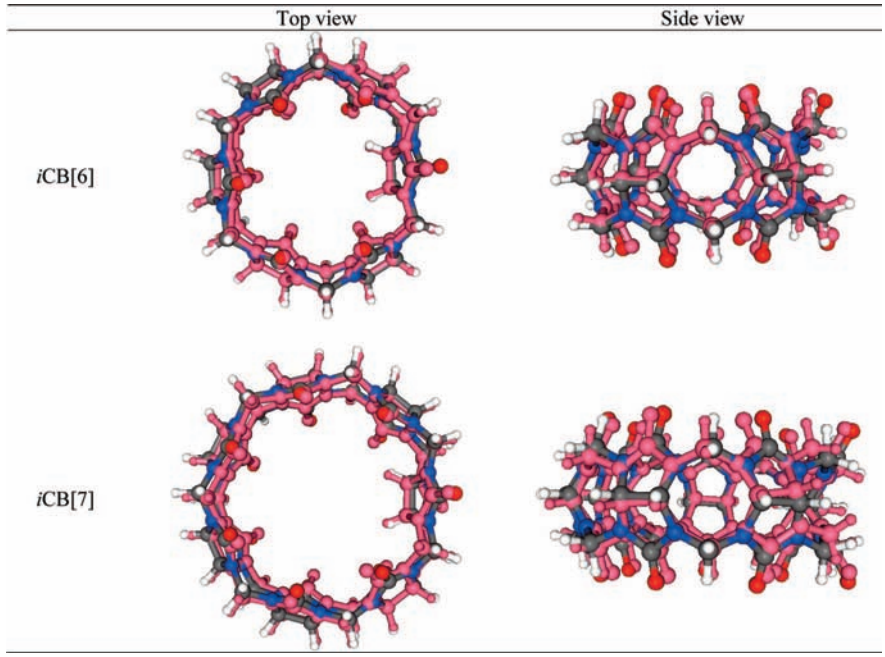

Figure 2. Superimposed geometries from the crystal structure and B3LYP calculations.

NMR spectra were also studied. The computational method used in this work is outlined below.

2. Computational Method

Geometry optimizations of inverted CB[*n*] using the density functional calculations incorporating Becke's three-parameter exchange with Lee, Yang, and Parr's (B3LYP) correlation functional[53,54] are performed employing the GAUSSIAN03 program.[55] The internally stored 6-31G(d) basis was used. The MESP, $V(\mathbf{r})$, is given by the classical expression:

$$V(\mathbf{r}) = \sum_{A=1}^{M} \frac{Z_A}{|\mathbf{r} - \mathbf{R}_A|} - \int \frac{\rho(\mathbf{r}')\mathrm{d}^3\mathbf{r}'}{|\mathbf{r} - \mathbf{r}'|} \qquad (1)$$

In the above equation, M is total number of nuclei in the molecule and Z_A defines the charge of the nucleus located at $\mathbf{R}_A$, with $\rho(\mathbf{r})$ being the electron density at location $\mathbf{r}$. The two terms in eq 1 refer to the bare nuclear potential and electronic contributions, respectively. Balance of these two terms brings about the effective localization of electron-rich regions in the molecular system.[56−61] The MESP topography is then mapped by examining the eigenvalues of the Hessian matrix at the point where the gradient $V(\mathbf{r})$ vanishes; the MESP critical points (CPs) were thereby located. A program developed in our laboratory was used to identify the CPs in the MESP topography.[62] The CPs are characterized in terms of an ordered pair (R, σ), where R and σ denote the rank and the signature (the sum of algebraic signs of the eigenvalues) of the Hessian matrix, respectively. These CPs can further be grouped into three sets, namely, (3, +3), (3, +1), and (3, −1). The (3, +3) CPs correspond to the local minima, whereas the (3, +1) and (3, −1) CPs are saddle points. These minima in the MESP topography represent potential binding sites for the electrophilic interactions. The program UNIVIS-2000 was employed for visualization of the MESP.[63] Frontier orbitals were analyzed by using the program MOLEKEL.[64,65] NMR chemical shifts (δ) were calculated by subtracting the nuclear magnetic shielding tensors for protons in the *i*CB[*n*] from that for the protons in tetramethylsilane (TMS) (as a reference) obtained from the gauge invariant atomic orbital (GIAO) method.[66] The effect of solvation on energetics

TABLE 1: Stabilization (in kJ mol^{-1}) of i^xCB[n] Enantiomers Relative to (i) the Lowest Energy Inverted CB[n] Enantiomers (ΔE_{Rel}) and (ii) the Corresponding CB[n] Homologue (ΔE_{Stab})[a]

	ΔE_{Rel}				ΔE_{Stab}				dipole moment
	gas phase	water	ethanol	THF	gas phase	water	ethanol	THF	gas phase
*i*CB[6]	0.0	0.0	0.0	0.0	4.2	28.7	27.7	23.0	7.1
*i*CB[7]	0.0	0.0	0.0	0.0	5.7	27.7	22.9	17.9	7.2
*i*CB[8]	0.0	0.0	0.0	0.0	−18.6	29.8	23.5	15.2	7.2
1,2-i^2CB[7]	61.6	59.9	67.0	59.5	72.2	115.7	118.2	98.3	13.4
1,3-i^2CB[7]	5.6	4.6	1.7	5.2	16.1	60.4	53.0	44.0	9.0
1,4-i^2CB[7]	0.0	0.0	0.0	0.0	10.5	55.8	51.2	38.9	3.2
1,2-i^2CB[8]	38.2	37.5	39.1	41.0	29.1	98.6	89.2	75.4	13.2
1,3-i^2CB[8]	1.0	2.2	2.5	1.5	−8.1	63.3	52.5	35.9	10.3
1,4-i^2CB[8]	0.0	0.0	0.0	0.0	−9.1	61.1	50.0	34.5	5.6
1,5-i^2CB[8]	0.2	0.6	0.3	−0.4	−9.0	61.6	50.4	34.0	0.2

[a] The dipole moments (in Debye) are also given.

of i^xCB[n] homologues as well as NMR chemical shifts therein was studied by using the self-consistent reaction field (SCRF) theory employing the polarizable continuum model (PCM) as implemented in the GAUSSIAN03 program.[67]

3. Results and Discussion

The atom numbering scheme in the monomer unit (glycouril) of the *i*CB[n] is displayed in Figure 1a. Atom type and numbering of hydrogen atoms in the inverted cucurbit[n]uril(s) are depicted in Figure 1b with 1,4-i^2CB[n] as an illustration. Thus, atoms in the inverted glycouril (depicted in red color) differ in their orientation compared to those in the rest of the monomer. In the inverted glycouril, the methine carbons (C_4 and C4′) and the corresponding hydrogen (H_2) direct toward the cavity while the ureido group (oxygens O_1) points away from the cavity. Atoms in the monomer unit nearest to the inverted glycouril unit orientated similar to those in CB[n] are designated by α. Similarly, atoms from succeeding monomer units are assigned notations β, γ, and δ. As displayed in Figure 1b, the star (★) denotes the atoms in glycouril of i^2CB[n] that are between two inverted units and possess a lesser number of monomers than those on the other side. The methylene protons pointing away from the cavity (H_1) are shown by the broken wedge lines, and H_2 are the methine protons. Finally, methylene protons represented by the wedge lines that point toward the *i*CB[n] portals are denoted as H_3. It should be remarked here that *i*CB[6] and *i*CB[7] have been isolated as intermediates during the synthesis of CB[n].[51] i^2CB[7] with two inverted glycouril units in CB[7] has also been conjectured. As a pursuance, the conformers possessing one (*i*CB[n], $n = 6-8$) and two (i^2CB[n], $n = 7, 8$) inverted monomer units of the corresponding CB[6] to CB[8] homologues have been considered. Stationary point geometries of *i*CB[6] and *i*CB[7] obtained from the present calculations and those from the X-ray crystal structures are superimposed on each other in Figure 2. Both the top and side views are shown. It is readily discernible from the superimposed geometries shown in the figure that the B3LYP optimized structures match well with those derived from the X-ray crystal data. A slight deviation of the *i*CB[7] optimized structure from its X-ray structure can be noticed, since the experimental *i*CB[7] structure refers to the complex with the guest tetrahydrofuran (THF) residing within the cavity.

Relative stabilization energies (ΔE_{Rel}) of different i^xCB[n] enantiomers are given in Table 1. A large separation of inverted glycouril units that minimizes the repulsions due to methine protons within the cavity is one of the factors contributing toward the enantiomer stability. Consequently, 1,4-i^2CB[n] turns out to be the lowest energy enantiomer in i^2CB[7] and i^2CB[8] as well. A comparison of stabilization energies (ΔE_{Stab}) of inverted CB[n] homologues and the corresponding CB[n] have shown that the *i*CB[8] and i^2CB[8] enantiomers, with an exception of the 1,2-i^2CB[8] enantiomer, are favored. The inversion of a glycouril in CB[6] and CB[7] engenders a destabilization of 4.2 and 5.7 kJ mol^{-1}, respectively. As opposed to this, *i*CB[8] is favored by −18.6 kJ mol^{-1} over CB[8]. The stabilization energy of the *i*CB[8] enantiomer is nearly twice that of 1,4-i^2CB[8] (−9.1 kJ mol^{-1}).

In order to gauge the influence of solvation on the energetics of i^xCB[n] enantiomers, the SCRF calculations incorporating the PCM model were carried out. Calculated ΔE_{Stab} values in water led to destabilization of *i*CB[n] by ∼28 kJ mol^{-1} over its CB[n] counterpart. As shown in Table 1, the i^2CB[n] enantiomers are largely destabilized compared to the *i*CB[n] homologues. Accordingly, for the 1,4-i^2CB[8] enantiomer, the stabilization energy amounting to 61.1 kJ mol^{-1} was noticed. Calculated ΔE_{Stab} in THF suggests a marginal preference for the 1,5-i^2CB[8] enantiomer (by 0.4 kJ mol^{-1}) over its 1,4-counterpart. The solvation by THF leads to the stabilization hierarchy *i*CB[6] < *i*CB[7] < *i*CB[8], with the ΔE_{Stab} values being 23.0, 17.9, and 15.2 kJ mol^{-1}, respectively.

The inverting of a glycouril unit(s) of CB[n] engender loss of symmetry of the CB[n] hosts and consequently renders a large dipole moment to the i^xCB[n] enantiomers displayed in Table 1. Enantiomers with an inverted glycouril result in a dipole moment as large as ∼7 D, whereas inverting of yet another glycouril unit imparts a dipole moment as large as ∼13.2 D to the 1,2-i^2CB[n] enantiomer. Dipole moments of these enantiomers decrease steadily with an increased separation of inverted units.

The MESP isosurface with $V = -157.5$ kJ mol^{-1} in the i^xCB[n] has been depicted in Figure 1S of the Supporting Information. The electron-rich regions suggest the binding sites for the interaction with the guest. Unlike in *i*CB[7] or *i*CB[8], the MESP isosurface encompasses the portals of *i*CB[6] entirely, which suggests that the interactions with the guest are largely electrostatic in nature.

A zero-valued MESP isosurface ($V = 0.0$ kJ mol^{-1}), utilized to gauge the shape of the i^xCB[n] cavities, is displayed in Figure 3. The negative potential inside the cavity of inverted CB[n] homologues (displayed for *i*CB[8] as an illustration) partly explains the affinity toward the electron deficient guest. The MESP isosurface within *i*CB[6] engenders a broken-sprocket-like cavity. An increase in the cavity size with an additional tooth per glycouril unit has been observed for the higher homologues. The *i*CB[n] cavities are strikingly similar and capable of selective binding of different guests. The 1,2-i^2CB[n]

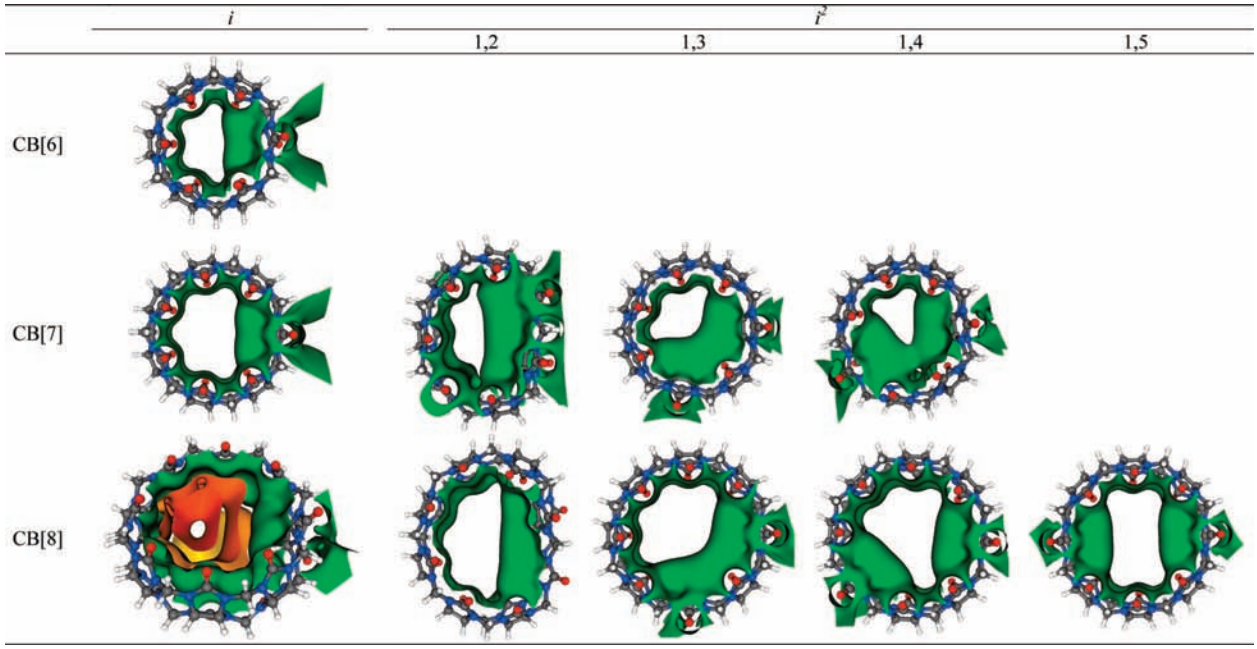

Figure 3. MESP isosurface ($V = 0.0$ kJ mol^{-1}) in inverted CB[*n*] homologues, displaying the cavity shapes. The negative potential present inside the cavity is as shown in the case of *i*CB[8].

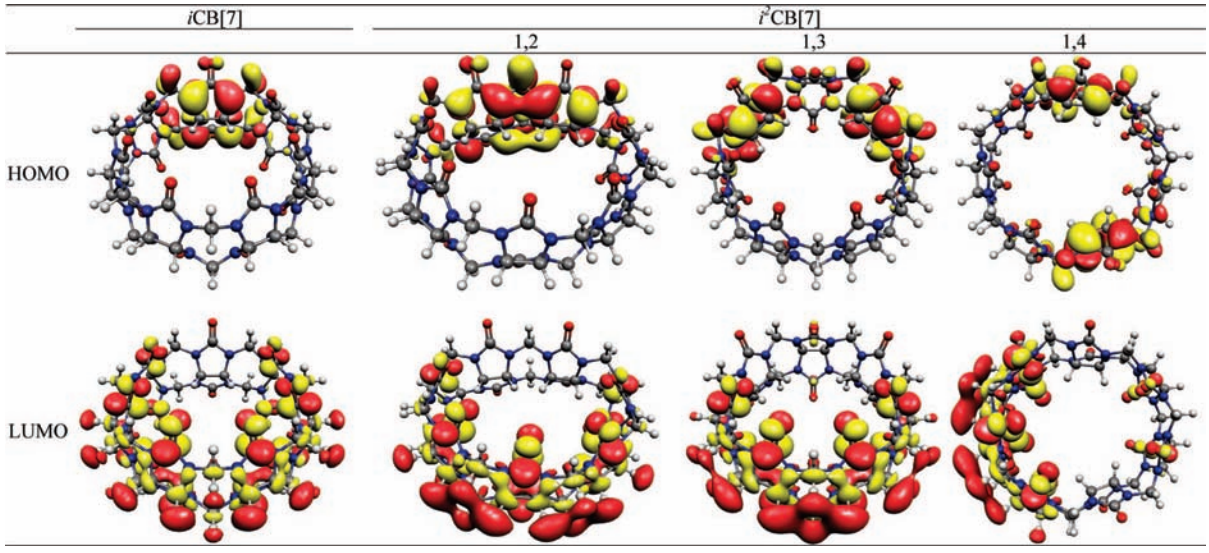

Figure 4. Frontier orbitals in inverted *i*^{x}CB[7] enantiomers. The HOMO is localized over the inverted glycouril(s).

TABLE 2: MESP Minima (in kJ mol^{-1}) near the Ureido Oxygens (x) and inside the Cavity (y) of Inverted CB[*n*] Homologues

							i^2CB[7]						i^2CB[8]							
	*i*CB[6]		*i*CB[7]		*i*CB[8]		1,2-		1,3-		1,4-		1,2-		1,3-		1,4-		1,5-	
	x	y	x	y	x	y	x	y	x	y	x	y	x	y	x	y	x	y	x	y
$\beta^{\star}$												−22.3						−32.8	−219.2	−42.0
$\alpha^{\star}$									−201.5		−214.6				−196.9		−207.4		−211.4	
i	−228.4	−52.5	−228.4	−5.3	−225.8	−2.6	−219.2	−34.1	−212.7		−212.7	−28.2	−216.6	−31.5	−211.4	−14.4	−214.3		−215.3	
α	−254.7		−238.9		−225.8		−223.2		−215.3		−217.3		−217.9	−30.2	−212.7		−211.4		−211.4	
β	−254.7	−31.5	−244.2	−47.3	−236.3	−59.1	−226.4	−15.8	−225.8	−32.2	−225.1	−32.8	−223.8	−68.3	−222.5	−47.3	−220.5	−45.9	−219.2	−42.0
γ	−254.7	−47.3	−244.2	−57.8	−238.9	−68.3	−220.5	−60.4		−39.4			−220.5	−70.9	−223.2	−56.4		−49.9		
δ				−61.7	−238.9	−72.9														

cavities also resemble a broken sprocket as noticed in case of the *i*CB[*n*] hosts. A different shape of the i^2CB[*n*] cavity results in varying separation between inverted glycourils. It should be remarked here that the 1,5-i^2CB[8] enantiomer leads to a nearly rectangular shaped cavity that may facilitate selective binding toward a planar guest. Thus, the cavity shape gauged from the MESP isosurface precludes the guest that binds tightly within the *i*^{x}CB[*n*] host.

The MESP topography in the *i*^{x}CB[*n*] hosts yields minima near the ureido oxygen (yellow) and inside the cavity (pink). Both the top and side views of these minima in the *i*CB[*n*] hosts are depicted in Figure 2S of the Supporting Information. The minima inside the cavity are located near the junction of two-glycouril units (small cavity formed by N_3 and N_5 nitrogens of monomer and N_3' and N_5' of other monomer). Thus, the effective cavity dimensions of *i*CB[*n*] at the portal and inside the cavity

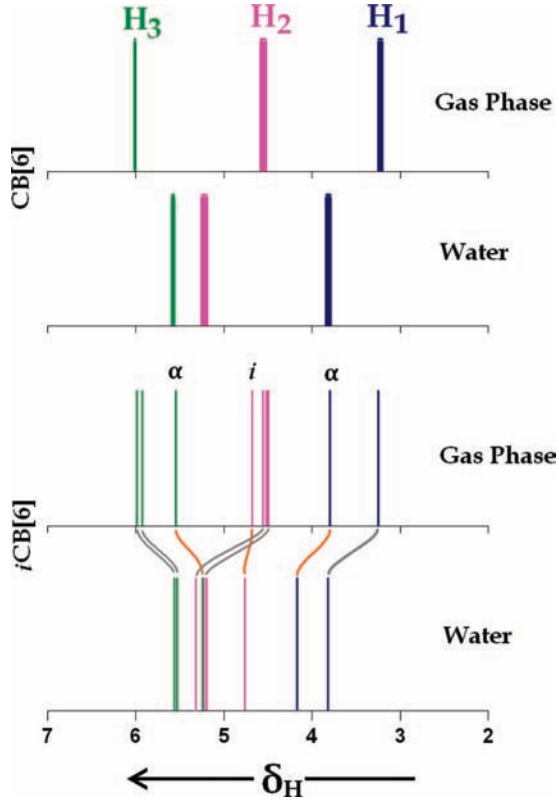

Figure 5. NMR chemical shifts δ_H of protons in CB[6] and *i*CB[6] enantiomers. The δ_H values are shifted significantly in water. Inverted methine (H_2) protons are less influenced in solvent.

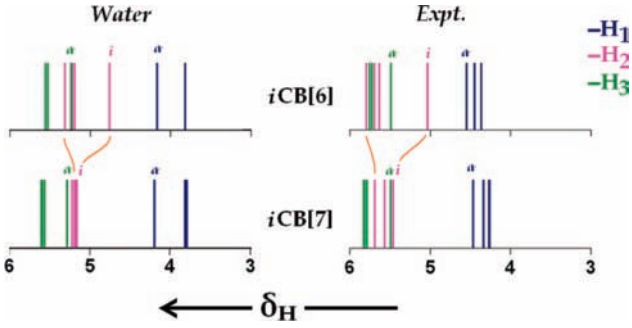

Figure 6. Comparison of δ_H values in *i*CBCB[6] and *i*CB[7] enantiomers calculated in water and observed in experiments.

noticed from the MESP topography are nearly the same. These MESP minima (in kJ mol^{-1}) near the ureido oxygens in a portal ("x") and those near nitrogen atoms ("y") are reported in Table 2. The reported values refer to the average electrostatic potential at the CPs of equivalent oxygens in both portals. The inverted unit yields the minima outside the cavity. It is further evident that the inverted glycouril oxygens engender the shallow minima. For example, in *i*CB[6], minima with -228.4 kJ mol^{-1} were located near inverted ureido oxygens, whereas those for the rest of the oxygens were identified with -254.7 kJ mol^{-1}. A large separation from the inverted glycouril endows the ureido oxygen to be more electron-rich as is evident from the MESP minima near the γ-oxygen of *i*CB[8] which turns out to be -238.9 kJ mol^{-1} while the α-oxygen exhibits minima with -225.8 kJ mol^{-1}. It should also be remarked here that, by increasing the number of glycouril units in *i*CB[*n*], MESP minima near the nitrogen ("y") become electron-rich, and thus, the γ-nitrogen of *i*CB[8] yields the MESP minima with $V = -68.3$ kJ mol^{-1} as compared to -47.3 kJ mol^{-1} in *i*CB[6]. It may, therefore, be inferred that on going from *i*CB[6] to *i*CB[8] the hydrophilicity at the portals decreases and the cavity becomes less hydrophobic.

As far as the i^2CB[*n*] enantiomers are concerned, the oxygens nearer to the inverted glycouril yield shallow minima as observed for the *i*CB[*n*] enantiomers. Moreover, with a large separation between the inverted glycouril units, the "x" and "y" CPs in i^2CB[8], shown in Figure 2S in the Supporting Information, become less electron-rich. In concurrence with this, the α* CPs in the 1,5-i^2CB[8] enantiomer are deeper while the β-"x" and β-"y" CPs exhibit shallow minima. Accordingly, the increasing number of glycourils between the two inverted units endows largely electron-rich ureido oxygens.

The interactions from the host can be analyzed from the charge distribution within the Frontier molecular orbitals. Frontier molecular orbitals in i^xCB[7] are displayed in Figure 4. It is transparent that the highest occupied molecular orbital (HOMO) has largely been localized near the inverted glycouril units. As opposed to this, the lowest unoccupied molecular orbital (LUMO) by and far is localized over the rest of noninverted glycouril units of i^xCB[*n*]. The complimentary electron-localization regions within the HOMO and LUMO may also be noticed in rest of the i^xCB[*n*] homologues depicted in Figure 3S of the Supporting Information.

^{1}H and ^{13}C chemical shifts in the NMR spectra of the i^xCB[*n*] enantiomers are calculated in the gas phase and with water as a solvent. The protons H_1, H_2, and H_3 of CB[*n*] hosts (without any inverted glycouril) in the gas phase yield the NMR signals near $\delta_H = 3.2$, 4.6, and 6.0 ppm, respectively.[43] The inverting of glycouril affects the δ_H values in CB[*n*] significantly. NMR spectra of CB[6] and *i*CB[6] are compared in this respect in Figure 5. As revealed from the figure, H_1 and H_3 protons bonded to the α-methylene carbon show distinct signals at 3.80 and 5.55 ppm, respectively, than those of the β, γ, or δ protons. It may further be noticed that the H_1 protons are downshifted while

TABLE 3: NMR Chemical Shifts in *i*^{x}CB[*n*] in the Gas Phase and in Water

		gas phase			water					gas phase			water		
*i*CB[*n*]		H_1	H_2	H_3	H_1	H_2	H_3	*i*^{2}CB[7]		H_1	H_2	H_3	H_1	H_2	H_3
*i*CB[6]	*i*		4.52			4.76		1,2-	*i*	4.48	4.95	5.41	4.67	5.23	5.14
	α	3.80	4.68	5.55	4.17	5.32	5.24		α	3.91	4.81	5.52	4.28	5.44	5.25
	β	3.25	4.56	5.93	3.84	5.20	5.53		*β*	3.30	4.42	5.95	3.90	5.13	5.56
	γ	3.25	4.50	5.99	3.82	5.23	5.56		*γ*	3.24	4.36	6.05	3.83	5.11	5.57
*i*CB[7]	*i*		4.91			5.17		1,3-	α★	3.85	4.65	5.58	4.22	5.30	5.28
	α	3.85	4.57	5.63	4.2	5.23	5.29		*i*		4.84			5.13	
	β	3.22	4.49	6.01	3.82	5.20	5.57		α	3.85	4.60	5.62	4.21	5.27	5.30
	γ	3.23	4.47	6.06	3.82	5.18	5.6		*β*	3.23	4.47	6.01	3.83	5.18	5.57
	δ	3.22		6.07	3.80		5.61		*γ*	3.21		6.04	3.80		5.59
*i*CB[8]	*i*		5.01			5.26		1,4-	*β*★	3.28		5.93	3.88		5.53
	α	3.83	4.51	5.63	4.18	5.21	5.29		α★	3.80	4.59	5.57	4.16	5.26	5.26
	β	3.24	4.41	6.06	3.83	5.16	5.59		*i*		4.68			5.00	
	γ	3.22	4.41	6.09	3.82	5.15	5.61		α	3.81	4.58	5.59	4.17	5.25	5.28
	δ	3.22	4.41	6.09	3.81	5.15	5.61		*β*	3.26	4.47	6.00	3.86	5.18	5.57

TABLE 4: B3LYP Calculated ^{13}C NMR Chemical Shifts in *i*^{x}CB[*n*] Homologues

							i^{2}CB[7]						*i*^{2}CB[8]							
	*i*CB[6]		*i*CB[7]		*i*CB[8]		1,2-		1,3-		1,4-		1,2-		1,3-		1,4-		1,5-	
	C_3	C_4	C_3	C_4	C_3	C_4	C_3	C_4	C_3	C_4	C_3	C_4	C_3	C_4	C_3	C_4	C_3	C_4	C_3	C_4
β★											52.9						54.3		54.2	71.1
α★									53.5	70.9	53.7	70.5			54.6	71.9	54.1	71.3	53.9	71.2
i		63.2		63.5		64.2	54.6	64.7		63.3		64.2	55.2	65.9		64.6		64.0		64.2
α	53.0	69.3	53.4	70.5	54.0	71.3	53.0	69.4	53.5	70.3	53.6	70.4	53.8	70.3	54.6	71.3	53.9	71.2	54.0	71.3
β	51.6	69.5	53.0	70.2	54.1	71.0	52.2	70.6	52.9	70.3	53.3	70.5	53.1	70.8	54.1	71.0	54.1	71.1	54.2	71.0
γ	52.3	69.3	53.3	70.3	54.3	71.1	54.7	71.7	53.5				54.8	72.0	54.4	71.1	54.4			
δ			53.1		54.2	71.0							55.5							
CB[*n*]	51.4	68.8	52.8	69.9	53.9	70.7	52.8	69.9	52.8	69.9	52.8	69.9	53.9	70.7	53.9	70.7	53.9	70.7	53.9	70.7

TABLE 5: ^{13}C NMR Chemical Shifts in *i*^{x}CB[*n*] Homologues in Water

							i^{2}CB[7]						*i*^{2}CB[8]							
	*i*CB[6]		*i*CB[7]		*i*CB[8]		1,2-		1,3-		1,4-		1,2-		1,3-		1,4-		1,5-	
	C_3	C_4	C_3	C_4	C_3	C_4	C_3	C_4	C_3	C_4	C_3	C_4	C_3	C_4	C_3	C_4	C_3	C_4	C_3	C_4
β★											52.1						53.4		53.3	70.1
α★									52.5	70.2	52.9	69.6			53.9	71.7	53.3	70.4	53.1	70.3
i		63.0		63.3		64.1	53.9	64.2		63.1		64.0	54.5	65.4		64.4		63.8		64.0
α	52.1	68.6	52.6	69.7	53.2	70.4	52.2	68.6	52.5	69.5	52.6	69.5	53.0	69.5	53.8	70.4	53.2	70.3	53.2	70.4
β	50.8	68.3	52.1	69.3	53.2	70.0	51.4	69.7	52.0	69.4	52.6	69.5	52.3	69.8	53.1	70.0	53.2	70.1	53.3	70.0
γ	51.4	68.9	52.3	69.3	53.3	70.0	53.7	70.7	52.5				53.8	70.9	53.4	70.1	53.4			
δ			52.2		53.2	70.0							54.5							
CB[*n*]	50.9	68.3	52.3	69.3	53.3	70.3	52.3	69.3	52.3	69.3	52.3	69.3	53.3	70.3	53.3	70.3	53.3	70.3	53.3	70.3

the H_3 protons exhibit an upshifted signal. Similarly, the H_2 protons of the inverted unit are deshielded and yield the NMR signal at $\delta_H = 4.52$ ppm. The gas phase NMR spectra of *i*CB[7] and *i*CB[8] are displayed in Figure 4S of the Supporting Information. It has clearly been noticed that the H_2 proton in the *i*CB[8] host is largely downshifted to $\delta_H = 5.01$ ppm. A downshift of the inverted H_2 increases steadily with the cavity size.

The NMR spectra of the CB[*n*] hosts possessing no inverted glycouril unit calculated in the solution (modeled via the SCRF) match well with the observed spectra.[43] In the following, we discuss the influence of solvation on the NMR signals of *i*^{x}CB[*n*] hosts. On solvation by water, the H_1 proton in *i*CB[6] bound to α-methylene carbon downshifts by 0.37 ppm while the downshift of ∼0.6 ppm was predicted for the corresponding *β* and *γ* protons. On the contrary, the α- as well as the *β*- (or *γ*-) H_3 proton exhibit δ_H signals which are upshifted by 0.31 and ∼0.4 ppm, respectively. The methine protons (H_2) yield a downshifted signal in aqueous solution. Here, the H_2 protons within the *i*CB[6] cavity are downshifted (0.24 ppm) and appear at $\delta_H = 4.76$ ppm, whereas the protons outside the cavity exhibit an ∼3 times larger downshift (0.64 ppm). Similar inferences may be drawn in the case of the *i*CB[7] and *i*CB[8] hosts. Moreover, NMR signals of α-H_1 (or α-H_3) are observed to be closer to those of the corresponding *β*, *γ*, or *δ* protons in aqueous solution. ^{1}H NMR chemical shifts in *i*CB[6] and *i*CB[7] in the presence of water are compared with those in the experimental ones in Figure 6.[51] An isolated signal of the inverted H_2 protons in *i*CB[6] can be observed. The distinct α-H_1 and α-H_3 protons are also noticed in both experimental as well as calculated spectra. On going from *i*CB[6] to *i*CB[7], the inverted H_2 (4.76 ppm) signal shows a prominent downshift of 0.41 ppm. Furthermore, the clustering of H_2 signals in the present calculations is consistent with the experimental spectra. The H_1

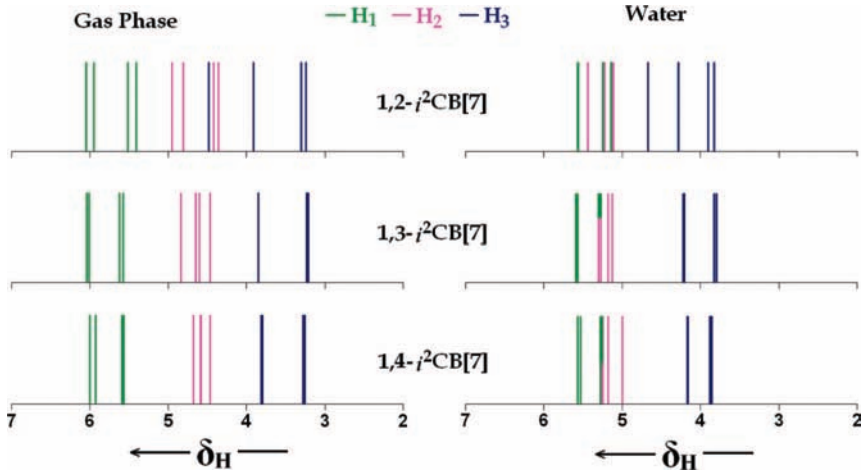

Figure 7. NMR chemical shifts δ_H in i^2CB[7] enantiomers in the gas phase and in water. H_2 signals appear close in 1,4-i^2CB[7].

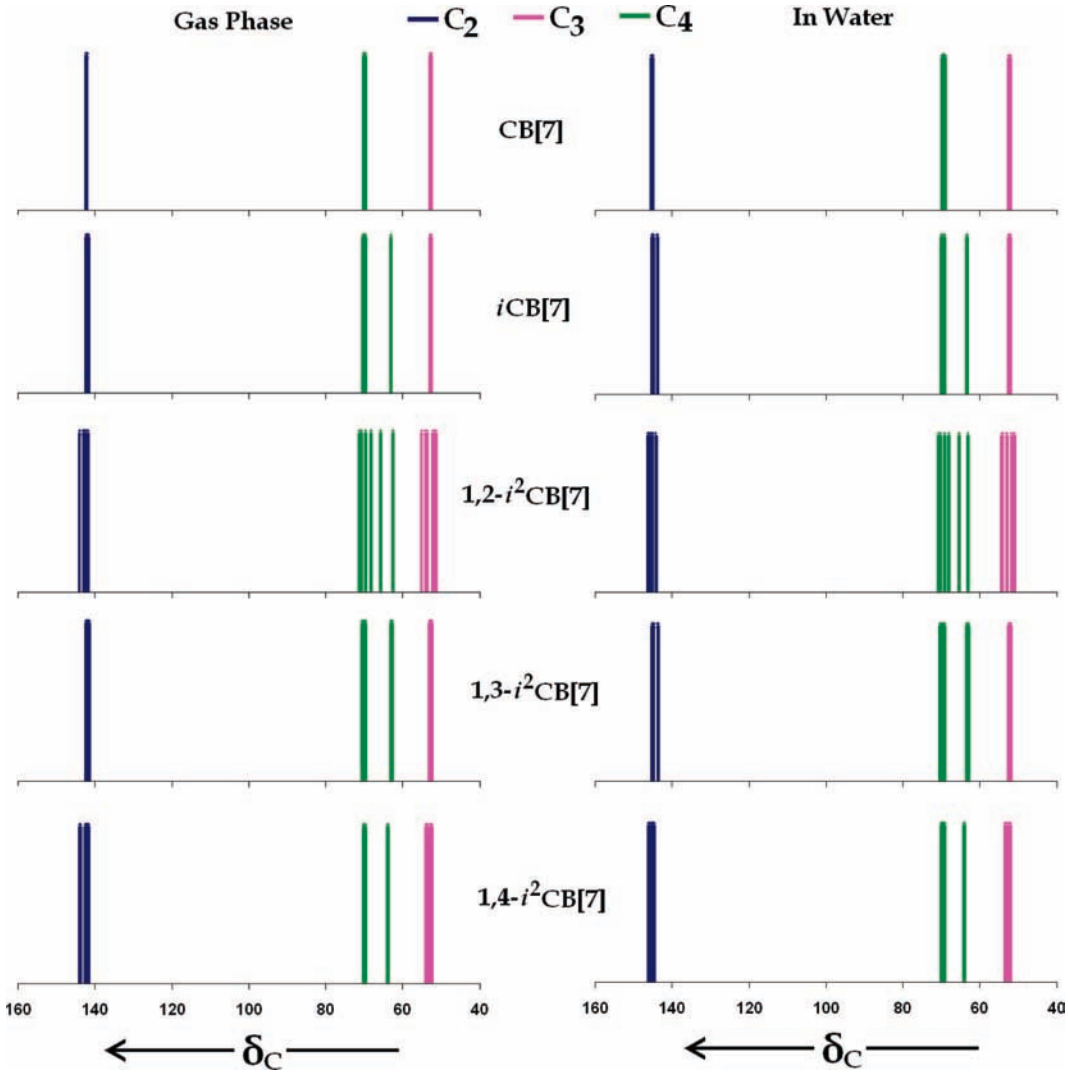

Figure 8. ^{13}C NMR chemical shifts of CB[n] and i^xCB[7] in the gas phase and in water. Inverted methine carbons (C_4) lead to clearly different signals compared to those in CB[7] enantiomers.

and H_3 protons turn out to be relatively less sensitive to the increase of cavity size. The calculated δ_H values predict a consistent upshift of ~0.4 ppm. NMR spectral patterns obtained from the SCRF calculations agree well with that observed in the experimental spectra.

The δ_H values of H_1, H_2, and H_3 in i^2CB[7] enantiomers in the gas phase and water are given in Table 3. On solvation, both i-H_1 and i-H_2 protons of the 1,2-i^2CB[7] enantiomer lead to a downshift of 0.20 and 0.28 ppm, respectively. The H_3 proton exhibits an upshifted signal at $\delta_H = 5.14$ ppm. The NMR spectra

of i^2CB[7] enantiomers in Figure 7 display relatively sparse signals in the gas phase. Here, the δ_H values of H_2 exhibit more crowded signals for the 1,4-i^2CB[7] enantiomer. As inferred earlier in *i*CB[*n*] hosts, solvation by water influences the H_1 and H_3 signals. An upshift in δ_H of H_3 leads to closely spaced lines in the NMR spectra. A shift in δ_H values of α-methylene and inverted methine protons is relatively small as discussed earlier for *i*CB[*n*] (cf. Table 4). The δ_H values of i^2CB[8] are displayed in Table 1S of the Supporting Information, and ^{1}H NMR spectra in the gas phase as well as in water are given in Figure 5S of the Supporting Information. The inferences drawn in the case of i^2CB[7] are also borne out by the i^2CB[8] enantiomers.

^{13}C chemical shifts of the methylene and methine carbons in i^xCB[*n*] and CB[*n*] are reported in Table 5. Calculated δ_C values of the inverted C_4 engender an upshifted signal at 63.2 ppm in *i*CB[6] compared to 68.8 ppm for CB[6] which possesss no inverted glycouril unit. This has been observed in the experiment, wherein an upshift of 8.2 ppm was noticed for inverted methine carbons appearing at $\delta_C = 62.8$ ppm.[51] The spectra of the *i*CB[*n*] homologues are compared in Figure 6S of the Supporting Information. In both CB[*n*] and *i*CB[*n*] homologues, an increase in cavity size engenders a larger downshift for the C_4. The cavity dimension, however, does not influence δ_C of the inverted methine carbons significantly. Accordingly, a downshift of ~0.3 ppm in *i*CB[7] has been noted for the inverted C_4 compared to that in *i*CB[6]. The methine carbon outside the cavity of *i*CB[7] exhibits a downshift (~1.1 ppm) and appears at $\delta_C = 69.9$ ppm. Calculated ^{13}C NMR spectra of CB[7] and i^xCB[7] in the gas phase are compared in Figure 8. As is transparent for the inverted CB[7] enantiomer, the methine carbons inside the cavity emerge with a distinct ^{13}C NMR signal from those predicted for CB[7]. It has further been inferred that the shift of the inverted methine carbon signals is less when the inverted glycourils are separated largely as may be noticed in 1,4-i^2CB[7]. The ^{13}C NMR spectra of *i*CB[*n*] and i^xCB[8], displayed in Figures 6S and 7S of the Supporting Information, also led to similar conclusions. ^{13}C NMR chemical shifts calculated in water are reported in Table 5. Solvation by water leads to an upshift of ~0.5 ppm for C_3 and C_4 in both *i*CB[*n*] and the i^2CB[*n*] hosts. SCRF calculations reveal that δ_C values of the inverted glycouril in *i*CB[*n*] and i^2CB[*n*] enantiomers are also less influenced by solvation. The results are summarized below.

4. Conclusions

Systematic investigations on the electronic structure, MESP topography, and ^{1}H NMR chemical shifts in *i*CB[*n*] and i^2CB[*n*] ($n = 6-8$) have been presented using the density functional theory with the B3LYP exchange correlation functional and the 6-31G(d) basis. The conclusions are summarized in the following. (i) *i*CB[8] is favored (by 18 kJ mol^{-1}) over CB[8] in the gas phase, whereas *i*CB[6] and *i*CB[7] are destabilized. The solvent influences the enantiomer stability, with THF engendering hierarchy of stabilization: *i*CB[6] < *i*CB[7] < *i*CB[8]. In the case of i^2CB[*n*], a larger separation of inverted glycourils yields the low energy 1,4-enantiomer. (ii) Different cavity shapes in i^xCB[*n*] can be gauged from the MESP isosurface; *i*CB[6] shows a half-sprocket-like cavity, with an extra tooth emerging with each additional glycouril for successive *i*CB[*n*] homologues. (iii) The corresponding i^2CB[7] and i^2CB[8] enantiomers yield cavities of different size which are strikingly similar. The different cavity shapes can be accomplished by varying the separation between inverted glycouril units of i^2CB[*n*] enantiomers, which may be useful for selective binding of different guests that fit inside the host cavity. (iv) MESP topography analysis reveals that minima near the ureido oxygens render electron-rich portals in the *i*CB[6] host over its *i*CB[7] or *i*CB[8] analogues. On going from *i*CB[6] to *i*CB[8], the hydrophilicity at the portals decreases whereas the cavity become less hydrophobic. (v) Frontier orbitals in i^xCB[*n*] reveal that the HOMO is largely localized on the inverted glycouril units only, whereas the LUMO extends itself only on rest of the *i*CB[*n*]. (vi) NMR chemical shifts predict that both the methylene protons near inverted monomer units and the methine proton within the cavity lead to distinct signals from those of the rest of the methylene or methine protons in i^xCB[*n*]. (vii) Solvation by water affects the NMR patterns in *i*CB[*n*], and crowding of lines from methine and corresponding methylene protons can be noticed. The δ_H values of the protons inside the cavity are, however, relatively less influenced by solvation.

To summarize, the present work may serve as an initial step toward the molecular level understanding of encapsulation of guests in the *i*CB[*n*] or i^2CB[*n*] cavities. The work can be extended to gain insights for the binding patterns of guests in other novel hosts as well.

Acknowledgment. The authors thank the Center for Network Computing, University of Pune, for providing computational facilities. S.P.G. is grateful to the University Grants Commission, New Delhi, for the major research project and University of Pune for disbursing the research grant under the potential excellence (UPE) scheme. R.V.P. acknowledges the Council of Scientific and Industrial Research (CSIR), New Delhi for a senior research fellowship.

Supporting Information Available: Figures showing MESP isosurface ($V = -157.5$ kJ mol^{-1}), MESP critical points in inverted i^2CB[*n*] enantiomers, Frontier orbitals in i^xCB[*n*], ^{1}H and ^{13}C NMR spectra of the i^xCB[*n*] enantiomers in the gas phase and in water, and table containing δ_H values in i^2CB[8] homologues. This material is available free of charge via the Internet at http://pubs.acs.org.

References and Notes

(1) Lagona, J.; Mukhopadhyay, P.; Chakrabarti, S.; Isaacs, L. *Angew. Chem., Int. Ed.* **2005**, *44*, 4844.
(2) Jeon, W. S.; Moon, K.; Park, S. H.; Chun, H.; Ko, Y. H.; Lee, J. Y.; Lee, E. S.; Samal, S.; Selvapalam, N.; Rekharsky, M. V.; Sindelar, V.; Sobransingh, D.; Inoue, Y.; Kaifer, A. E.; Kim, K. *J. Am. Chem. Soc.* **2005**, *127*, 12984.
(3) Buschmann, H.-J.; Jansen, K.; Schollmeyer, E. *Thermochim. Acta* **1998**, *317*, 95.
(4) Buschmann, H.-J.; Jansen, K.; Schollmeyer, E. *Thermochim. Acta* **2000**, *346*, 33.
(5) Ong, W.; Kaifer, A. E. *Angew. Chem., Int. Ed.* **2003**, *42*, 2164.
(6) Ong, W.; Kaifer, A. E. *J. Org. Chem.* **2004**, *69*, 1383.
(7) Sun, S.; Zhang, R.; Andersson, S.; Pan, J.; Åkermark, B.; Sun, L. *Chem. Commun.* **2006**, 4195.
(8) Ling, Y.; Wang, W.; Kaifer, A. E. *Chem. Commun.* **2007**, 610.
(9) Ling, Y.; Mague, J. T.; Kaifer, A. E. *Chem.— Eur. J.* **2007**, *13*, 7908.
(10) Jansen, K.; Wego, A.; Buschmann, H.-J.; Schollmeyer, E. *Vom Wasser* **2000**, *95*, 229.
(11) Wagner, D.; Stojanovic, N.; Day, A. I.; Blanch, R. J. *J. Phys. Chem. B* **2003**, *107*, 10741.
(12) Choi, S.; Park, S. H.; Ziganshina, A. Y.; Ko, Y. H.; Lee, J.; W.; Kim, K. *Chem. Commun.* **2003**, 2176.
(13) Wei, F.; Liu, S.-M.; Xu, L.; Cheng, G.-Z.; Wu, C.-T.; Feng, Y.-Q. *Electrophoresis* **2005**, *26*, 2214.
(14) Ong, W.; Kaifer, A. E. *Organometallics* **2003**, *22*, 4181.
(15) Feng, K.; Wu, L.-Z.; Zhang, L.-P.; Tung, C.-H. *Dalton Trans.* **2007**, 3991.
(16) Wheate, N. J.; Taleb, R. I.; Krause-Heuer, A. M.; Cook, R. L.; Wang, S.; Higgins, V. J.; Aldrich-Wright, J. R. *Dalton Trans.* **2007**, 5055.

(17) Sobransingh, D.; Kaifer, A. E. *Langmuir* **2006**, *22*, 10540.
(18) Buschmann, H.-J.; Jansen, K.; Meschke, E.; Schollmeyer, E. *J. Solution Chem.* **1998**, *27*, 135.
(19) Buschmann, H.-J.; Schollmeyer, E.; Mutihac, L. *Thermochim. Acta* **2003**, *399*, 203.
(20) Heitmann, L. M.; Taylor, A. B.; John Hart, P.; Urbach, A. R. *J. Am. Chem. Soc.* **2006**, *128*, 12574.
(21) Jon, S. Y.; Ko, Y. H.; Park, S. H.; Kim, H.-J.; Kim, K. *Chem. Commun.* **2001**, 1938.
(22) Lee, J. W.; Kim, K.; Choi, S.; Ko, Y. H.; Sakamoto, S.; Yamaguchi, K.; Kim, K. *Chem. Commun.* **2002**, 2692.
(23) Wang, R.; Yuan, L.; Macartney, D. H. *J. Org. Chem.* **2006**, *71*, 1237.
(24) Wu, X.-L.; Luo, L.; Lei, L.; Liao, G.-H.; Wu, L.-Z.; Tung, C.-H. *J. Org. Chem.* **2008**, *73*, 491.
(25) Pattabiraman, M.; Kaanumalle, L. S.; Natarajan, A.; Ramamurthy, V. *Langmuir* **2006**, *22*, 7605.
(26) Maddipatla, M. V. S. N.; Kaanumalle, L. S.; Natarajan, A.; Pattabiraman, M.; Ramamurthy, V. *Langmuir* **2007**, *23*, 7545.
(27) Lei, L.; Luo, L.; Wu, X.-L.; Liao, G.-H.; Wu, L.-Z.; Tung, C.-H. *Tetrahedron Lett.* **2008**, *49*, 1502.
(28) Kolb, H. C.; Finn, M. G.; Sharpless, K. B. *Angew. Chem., Int. Ed.* **2001**, *40*, 2004.
(29) Tuncel, D.; Steinke, J. H. G. *Macromolecules* **2004**, *37*, 288.
(30) Tuncel, D.; Steinke, J. H. G. *Chem. Commun.* **2002**, 496.
(31) Balzani, V.; Credi, A.; Raymo, F. M.; Stoddart, J. F. *Angew. Chem., Int. Ed.* **2000**, *39*, 3348.
(32) Corma, A.; García, H.; Montes-Navajas, P.; Primo, A.; Calvino, J. J.; Trasobares, S. *Chem.—Eur. J.* **2007**, *13*, 6359.
(33) Lee, J. W.; Samal, S.; Selvapalam, N.; Kim, H.-J.; Kim, K. *Acc. Chem. Res.* **2003**, *36*, 621.
(34) Mock, W. L. *Top. Curr. Chem.* **1995**, *175*, 1.
(35) Kim, K. *Chem. Soc. Rev.* **2002**, *31*, 96.
(36) Jeon, Y. J.; Bharadwaj, P. K.; Choi, S. W.; Lee, J. W.; Kim, K. *Angew. Chem., Int. Ed.* **2002**, *41*, 4474.
(37) Rauwald, U.; Scherman, O. A. *Angew. Chem., Int. Ed.* **2008**, *47*, 3950.
(38) Sindelar, V.; Cejas, M. A.; Raymo, F. M.; Chen, W.; Parker, S. E.; Kaifer, A. E. *Chem.—Eur. J.* **2005**, *11*, 7054.
(39) Ko, Y. H.; Kim, E.; Hwang, I.; Kim, K. *Chem. Commun.* **2007**, 1305.
(40) Kim, J.; Jung, I.-S.; Kim, S.-Y.; Lee, E.; Kang, J.-K.; Sakamoto, S.; Yamaguchi, K.; Kim, K. *J. Am. Chem. Soc.* **2000**, *122*, 540.
(41) Day, A. I.; Arnold, A. P.; Blanch, R. J.; Snushall, B. *J. Org. Chem.* **2001**, *66*, 8094.
(42) Day, A. I.; Blanch, R. J.; Arnold, A. P.; Lorenzo, S.; Lewis, G. R.; Dance, I. *Angew. Chem., Int. Ed.* **2002**, *41*, 275.
(43) Pinjari, R. V.; Gejji, S. P. *J. Phys. Chem. A* **2008**, *112*, 12679.
(44) Carlqvist, P.; Maseras, F. *Chem. Commun.* **2007**, 748.
(45) Buschmann, H.-J.; Wego, A.; Zielesny, A.; Schollmeyer, E. *J. Inclusion Phenom. Macrocyclic Chem.* **2006**, *54*, 241.
(46) Pichierri, F. *J. Mol. Struct. (THEOCHEM)* **2006**, *765*, 151.
(47) Pichierri, F. *Chem. Phys. Lett.* **2004**, *390*, 214.
(48) Oh, K. S.; Yoon, J.; Kim, K. S. *J. Phys. Chem. B* **2001**, *105*, 9726.
(49) Chakraborty, A.; Wu, A.; Witt, D.; Lagona, J.; Fettinger, J. C.; Isaacs, L. *J. Am. Chem. Soc.* **2002**, *124*, 8297.
(50) Wu, A.; Chakraborty, A.; Witt, D.; Lagona, J.; Damkaci, F.; Ofori, M. A.; Chiles, J. K.; Fettinger, J. C.; Isaacs, L. *J. Org. Chem.* **2002**, *67*, 5817.
(51) Isaacs, L.; Park, S.-K.; Liu, S.; Ko, Y. H.; Selvapalam, N.; Kim, Y.; Kim, H.; Zavalij, P. Y.; Kim, G.-H.; Lee, H.-S.; Kim, K. *J. Am. Chem. Soc.* **2005**, *127*, 18000.
(52) Liu, S.; Kim, K.; Isaacs, L. *J. Org. Chem.* **2007**, *72*, 6840.
(53) Becke, A. D. *Phys. Rev. A* **1988**, *38*, 3098.
(54) Lee, C.; Yang, W.; Parr, R. G. *Phys. Rev. B* **1988**, *37*, 785.
(55) Frisch, M. J.; Trucks, G. W.; Schlegel, H. B.; Scuseria, G. E.; Robb, M. A.; Cheeseman, J. R.; Montgomery, J. A., Jr.; Vreven, T.; Kudin, K. N.; Burant, J. C.; Millam, J. M.; Iyengar, S. S.; Tomasi, J.; Barone, V.; Mennucci, B.; Cossi, M.; Scalmani, G.; Rega, N.; Petersson, G. A.; Nakatsuji, H.; Hada, M.; Ehara, M.; Toyota, K.; Fukuda, R.; Hasegawa, J.; Ishida, M.; Nakajima, T.; Honda, Y.; Kitao, O.; Nakai, H.; Klene, M.; Li, X.; Knox, J. E.; Hratchian, H. P.; Cross, J. B.; Bakken, V.; Adamo, C.; Jaramillo, J.; Gomperts, R.; Stratmann, R. E.; Yazyev, O.; Austin, A. J.; Cammi, R.; Pomelli, C.; Ochterski, J. W.; Ayala, P. Y.; Morokuma, K.; Voth, G. A.; Salvador, P.; Dannenberg, J. J.; Zakrzewski, V. G.; Dapprich, S.; Daniels, A. D.; Strain, M. C.; Farkas, O.; Malick, D. K.; Rabuck, A. D.; Raghavachari, K.; Foresman, J. B.; Ortiz, J. V.; Cui, Q.; Baboul, A. G.; Clifford, S.; Cioslowski, J.; Stefanov, B. B.; Liu, G.; Liashenko, A.; Piskorz, P.; Komaromi, I.; Martin, R. L.; Fox, D. J.; Keith, T.; Al-Laham, M. A.; Peng, C. Y.; Nanayakkara, A.; Challacombe, M.; Gill, P. M. W.; Johnson, B.; Chen, W.; Wong, M. W.; Gonzalez, C.; Pople, J. A. *Gaussian 03*, revision C.02; Gaussian, Inc.: Wallingford, CT, 2004.
(56) Politzer, P. *Chemical Applications of Atomic and Molecular Electrostatic Potentials*; Politzer, P., Ed.; Plenum: New York, 1981.
(57) Tomasi, J.; Bonnacorsi, R.; Cammi R. In *Theoretical Models of Chemical Bonding*; Maksic, Z. B., Ed.; Springer: Berlin, Heidelberg, New York, 1991; Vol. 4, p 228.
(58) Bonaccorsi, R.; Scrocco, E.; Tomasi, J. *J. Chem. Phys.* **1970**, *52*, 5270.
(59) Bonaccorsi, R.; Scrocco, E.; Tomasi, J. *Theor. Chim. Acta* **1979**, *52*, 113.
(60) Náray-Szabó, G.; Ferenczy, G. G. *Chem. Rev.* **1995**, *95*, 829.
(61) Gadre, S. R.; Kulkarni, S. A.; Shrivastava, I. H. *J. Chem. Phys.* **1992**, *31*, 5253.
(62) Balanarayan, P.; Gadre, S. R. *J. Chem. Phys.* **2003**, *119*, 5037.
(63) Limaye, A. C.; Gadre, S. R. *Curr. Sci.* **2001**, *80*, 1298.
(64) Flükiger, P.; Lüthi, H. P.; Portmann, S.; Weber, J. *MOLEKEL*, version 4.3; Swiss Center for Scientific Computing: Manno, Switzerland, 2000—2002.
(65) Portmann, S.; Lüthi, H. P. MOLEKEL: An Interactive Molecular Graphics Tool. *Chimia* **2000**, *54*, 766.
(66) Wolinski, K.; Hilton, J. F.; Pulay, P. *J. Am. Chem. Soc.* **1990**, *112*, 8251.
(67) Miertus, S.; Scrocco, E.; Tomasi, J. *Chem. Phys.* **1981**, *55*, 117.

JP809293S